REPORT | EXOPLANETS

A compositional link between rocky exoplanets and their host stars

Stars and planets both form by accreting material from a surrounding disk. Because they grow from the same material, theory predicts that there should be a relationship between their compositions. In this study, we search for a compositional link between rocky exoplanets and their host stars. We estimate the iron-mass fraction of rocky exoplanets from their masses and radii and compare it with the compositions of their host stars, which we assume reflect the compositions of the protoplanetary disks. We find a correlation (but not a 1:1 relationship) between these two quantities, with a slope of >4, which we interpret as being attributable to planet formation processes. Super-Earths and super-Mercuries appear to be distinct populations with differing compositions, implying differences in their formation processes.

Vardan Adibekyan [1,2] *, Caroline Dorn [3], Sérgio G. Sousa [1], Nuno C. Santos [1,2], Bertram Bitsch [4], Garik Israelian [5,6], Christoph Mordasini [7], Susana C. C. Barros [1,2], Elisa Delgado Mena [1], Olivier D. S. Demangeon [1,2], João P. Faria [1,2], Pedro Figueira [8,1], Artur A. Hakobyan [9], Mahmoudreza Oshagh [5,6], Bárbara M. T. B. Soares [1,2], Masanobu Kunitomo [10], Yoichi Takeda [11,12], Emiliano Jofré [13,14,15], Romina Petrucci [14,15], Eder Martioli1 [16,17]

Characterizing the interiors of rocky exoplanets requires measurements of both theirmass and radius. These parameters are usually provided by a combination of two techniques: planetary radius is determined via transit observations, and planetary mass via radial velocity (RV) measurements. The derivation of these parameters relies on properties of the host stars, so it is limited by the precision with which those are measured. Exoplanets orbiting stars that are similar to the Sun [i.e., F, G, or K (FGK) spectral types] benefit from the precise characterization that is possible for their host stars ([1]).

We consider a set of 32 low-mass exoplanets (planet mass, M, of <10 Earth masses, $M_\oplus$) orbiting 27 FGK stars with uncertainties in both planetmass and radius of <30%(2). Above ~4$M_\oplus$, the distribution of these planets on a mass-radius diagram shows an apparent gap between two populations (Fig. 1). This gap has been interpreted as the separation between rocky exoplanets and gas-rich mini-Neptunes (3-7). Our goal is to investigate how the properties of the rocky planets depend on the composition of their host stars. To this end, we discard the planets above the radius gap in Fig. 1, leaving 22 planets without substantial water or gas-rich envelopes, that is, rocky planets.

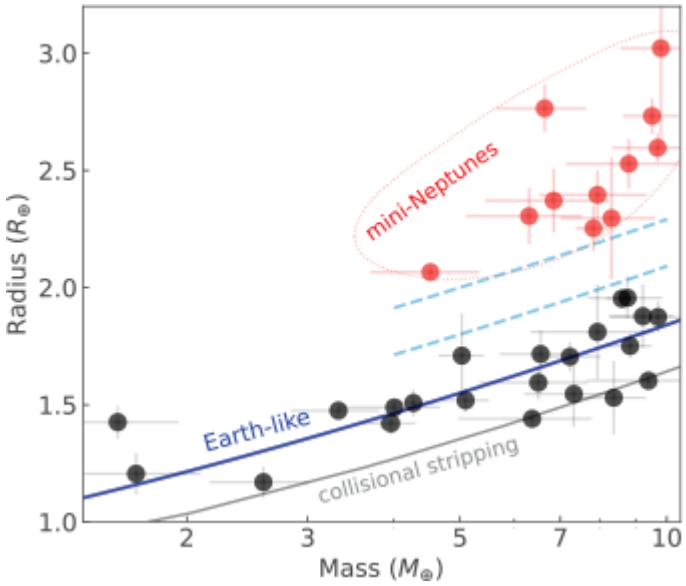

Fig. 1. Mass-radius diagram for the rocky planets in our sample. All planets in our sample have masses below 10 $M_\oplus$ and mass and radius uncertainties of <30%. The radii of the planets are given in Earth radii, $R_\oplus$. The light-blue dashed curves, drawn by eye, indicate the location of the radius gap that separates the mini-Neptunes with gaseous envelopes (red circles) from the planets without gaseous envelopes (black circles). The solid blue curve shows the mass-radius relationship expected for Earth-like composition (32% Fe + 68% $MgSiO_3$) (18). The gray solid curve marks the minimum planetary radius predicted by a collisional stripping (giant impact) model (23). All error bars show one standard deviation.

The abundances of elements in the atmospheres of main-sequence stars reflect their bulk composition (except the lightest elements) within a few percent (8), which meteorite measurements have shown to be valid for the Sun (9). Theory predicts that the Fe/Si and Mg/Si abundance ratios in stars and planets remain very similar during the planet formation process (10-12). The atmospheric abundances of refractory elements (such as

Mg, Si, and Fe) of solar-type stars are therefore considered a proxy of the composition of the initial protoplanetary disk (13, 14).

We analyzed spectra of 21 host stars of the selected planets (HD 80653 does not have an available spectrum) and measured their atmospheric chemical compositions (2). We determined the abundances of Mg, Si, and Fe in the host stars, which are the major rock-forming elements (15). We then inserted these abundances into a simple stoichiometric model (16, 17) to estimate the iron-to-silicate mass fraction ($f_{\mathrm{iron}}^{\mathrm{star}}$) of protoplanetary disks. For the protosolar disk, this model predicts $f_{\mathrm{iron}}^{\mathrm{Sun}}$ of 33.2 ± 1.7%, which is consistent with the iron content of Earth (~32%), Venus (~32%), and Mars (~30%) but differs from that of Mercury (~70%) (2).

At a given mass, the rocky planets in our sample have a dispersion in radius around the curve expected for Earth-like composition (Fig. 1). To investigate whether the densities of these planets are linked to the primordial composition of the protoplanetary disk, Fig. 2 shows the planet density, ρ, normalized to that expected for an Earth-like composition $\rho_{\mathrm{Earth\text{-}like}}$ (18) as a function of $f_{\mathrm{iron}}^{\mathrm{star}}$. The normalization accounts for planets with different masses having different densities even with the same composition, owing to compression. We find a relationship between these two quantities, indicating that the final planetary density is a function of the composition of the protoplanetary disk. We performed an orthogonal distance regression (ODR) analysis to quantify the relationship and then used *t* test statistics to assess its significance, finding that the observed correlation is statistically significant, with a *P* value of ~7 × 10–6 (2).

Because the normalized density is calculated from the observed properties of the planets, whereas $f_{\mathrm{iron}}^{\mathrm{star}}$ is inferred from the host star composition, this trend provides observational evidence for a compositional link between rocky exoplanets and their host stars. Rocky planets therefore preserve information about the composition of the protoplanetary disk in which they formed.

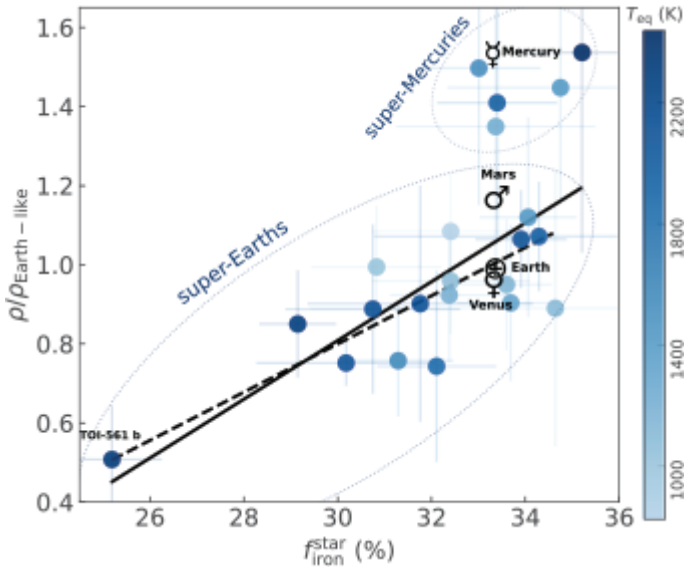

Fig. 2. Densities of rocky planets as a function of iron fraction. The measured density of each planet was normalized by the expected density of an Earth-like composition at that mass (**18**) (Fig. 1). The iron-mass fraction was calculated from the elemental abundances of the host star. The rocky planets in the Solar System are indicated with their respective symbols in black; these all have the same iron fraction because it was derived from the abundances of the Sun, not measured directly from the planets. The black solid and dashed lines show the correlation for the full sample and for the sample after excluding the five potential super-Mercuries, respectively. The Solar System planets are not included in the linear regressions. The exoplanet symbols (blue circles) are color coded by the equilibrium temperature of the planets to search for possible trends. No color gradient is visible. All error bars show one standard deviation.

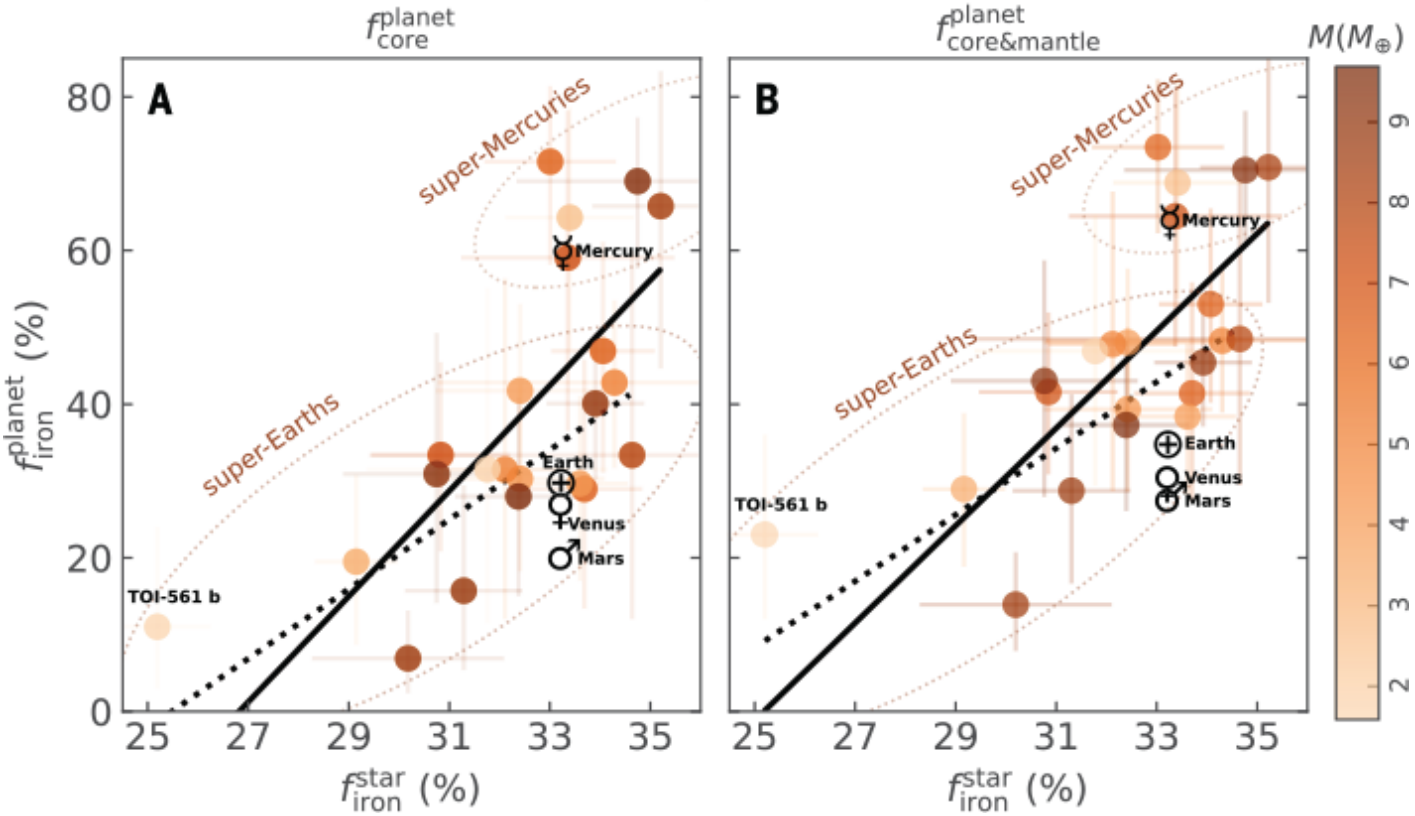

Fig. 3. Iron contents of rocky planets. The iron-mass fraction of the protoplanetary disk, estimated from the host star abundances ( ), is plotted as a function of the iron-mass fraction inferred from the planet's mass and radius ( ), as in Fig. 2. The values are shown for two assumptions: **(A)** All iron resides in the core only or **(B)** iron is present in both the mantle and core. The color bar indicates the mass of the planets. Symbols and line styles are the same as in Fig. 2. The error bars of show one standard deviation. The error bars of cover the interval between the 16th and the 84th percentiles.

Although Fig. 2 shows a correlation, it is evident that for a given f^{star}_{iron}, rocky planets can have a range of densities. The observed scatter is compatible with the average uncertainty of $\rho/\rho_{Earth\text{-}like}$. We nevertheless tested whether part of this dispersion could have an astrophysical origin. The size, and therefore density, of planets could be influenced by the flux of high-energy photons that the planets receive from their host stars (6).

Extreme irradiation from the host star can lead to atmospheric escape from low-mass planets, with a substantial impact on the evolution of their bulk composition (19). However, we found no correlation between the normalized density of the planets and their equilibrium temperature, T_{eq} (Fig. 2). Assuming that these planets have

maintained a constant T_{eq} since their formation, this lack of correlation suggests that for rocky planets, T_{eq} does not have a dominant impact on their radius. Alternatively, a radial oxidation gradient in the protoplanetary disks might lead to a correlation between orbital distance and composition and therefore also to a correlation between orbital distance and planet density (20). However, we also found no correlation between $\rho/\rho_{Earth\text{-}like}$ and the orbital distance of the planets (fig. S1).

We compared the iron-mass fraction of the planets with the iron-mass fraction of the protoplanetary disk, estimated from the host star composition. Using planet interiormodels (18), we calculated the possible iron-mass fraction of each planet (f_{iron}^{planet}) using only their mass and radius, without incorporating any constraints from the host star composition. We considered two scenarios: (i) iron is present only in the core or (ii) iron is present both in the core and mantle of each planet. Figure 3 shows the resulting relationship between f_{iron}^{planet} and f_{iron}^{star}, which indicates a correlation between those quantities for both scenarios. We again applied ODR and a *t* test, finding that the correlation is statistically significant (*P* value of ~2×10^{-5}). However, the planets span a wider range of iron-mass fractions than their host stars. The overall distribution of the coremass fraction (which can be related to the iron-mass fraction) of rocky planets has been shown to be wider than the overall distribution expected from the exoplanet host stars' composition (21).

It has been suggested that the iron fraction in planets can be increased relative to the protostellar value if the planets formed close to rocklines (regionswhere refractory material condenses or sublimates) (22). In this model, the enhancement in iron, however, is not high enough to explain the amount of iron in Mercury. This effect could explain the generally higher values of f_{iron}^{planet} compared with f_{iron}^{star}. The trend we find in Fig. 3 suggests that if this effect operates, it must depend on the stellar iron-mass fraction, such that stars with higher iron fraction have a larger rockline effect.

We identify a group of five planets (K2-38 b, K2-106 b, K2-229 b, Kepler-107 c, and Kepler-406 b) in Fig. 3 with a higher iron content than the rest of the planets. These five planets appear to be higher-mass analogs of Mercury, so we refer to them as super-Mercuries, a term previously proposed (23) by analogywith super-Earth, meaning planets with Earth-like compositions but higher masses. Several mechanisms of planet formation and evolution have been proposed to produce high-density and high-$f_{\text{iron}}^{\text{planet}}$ super-Mercury planets (24). The five super-Mercuries we identify have a wide range of masses, unlike the concentration around ~5 $M_{\oplus}$ predicted by simulations of giant impacts (23). We suggest that a giant impact alone is not responsible for the high density of super-Mercuries. Planet formation simulations that incorporate collisions are unable to produce the highest-density super-Mercuries (25). There is a possible gap in the $f_{\text{iron}}^{\text{planet}}$ and rEarth-like plane (Fig. 3) between super-Mercuries and super-Earths; we expect a continuous distribution from collisional stripping, given its stochastic nature.

Although we find only five super-Mercuries, they all orbit stars with high $f_{\text{iron}}^{\text{star}}$ (meaning an overabundance of Fe relative to Mg and Si) and high iron abundance (table S3),which is a proxy for the overall content of heavy elements in stars. The first trend may suggest that the mechanism responsible for the overabundance of iron in these planets is related to the composition of the protoplanetary disk. The second trend could imply a more efficient planet formation, leading to a formation of multiple planets and resulting in frequent collisions. We suggest that both iron enrichment (22) and collisional mantle stripping (25) may need to be invoked to produce an iron enrichment in the general planet population and explain the presence of super-Mercuries.

Because the super-Mercuries may have an unusual origin and/or evolution, we investigated whether our findings still apply if we exclude them from our sample (2). We find that the $f_{\text{iron}}^{\text{planet}}$ - $f_{\text{iron}}^{\text{star}}$ correlation remains significant (P value of <10–4) for just the sample of super-Earths (Fig. 3) but shifts the slope to lower values (tables S6 and S7). The difference in the slopes is, however, within the uncertainties: 6.3 ± 1.2 against 4.3 ± 0.8 for the case of

$f_{\text{core\&mantle}}^{\text{planet}}$

. In addition, we found that the Fe/(Mg + Si) abundance ratio estimated for these planets correlates with the Fe/(Mg + Si) ratio of their host stars (see the supplementary text section in the supplementary materials). Our results show a non–one-to-one relationship with a slope greater than 1 (supplementary text).

All but one of the stars in our sample are members of the Milky Way's thin disk. The exception is the ultrashort-period planet TOI-561 b, which orbits a metal-poor star in the thick disk; it was previously found to have an unusually low density (**26**). Figures 2 and 3 show that the low density of this planet is consistent with the general trend and dispersion we find for the entire sample. Theory predicts that planets orbiting around metalpoor thick disk and halo stars should have low iron-mass fractions (**17**).

Several previous studies have sought links between the composition of low-mass planets and their host stars. However, they were based either on single planetary systems (**27, 28**), on a small sample of planets (16, 21, 24), or on a statistical comparison of the overall populations (**21**). Owing to these limitations, none of those studies found a strong correlation.

The stellar abundances of major rock-forming elements, such as Fe, Mg, and Si, are commonly used to infer the bulk compositions of rocky planets (**13, 14**), including those in different stellar populations of the Milky Way (**17, 29**). Our results provide support for the assumptions made in those studies. The observed correlation we find between

$f_{\text{iron}}^{\text{planet}}$

and

$f_{\text{iron}}^{\text{star}}$

has a slope steeper than 1 (

$f_{\text{iron}}^{\text{planet}}$

is larger than

$f_{\text{iron}}^{\text{star}}$

); we interpret this as indicating that the composition of the protoplanetary disk (which varieswith time and location) influences the resulting composition of planets in a nonlinear fashion.

1Instituto de Astrofísica e Ciências do Espaço, Universidade do Porto, Centro de Astrofísica da Universidade do Porto, 4150-762 Porto, Portugal.

2Departamento de Física e Astronomia, Faculdade de Ciências, Universidade do Porto, 4169-007 Porto, Portugal.

3Institute for Computational Science, University of Zurich, CH-8057 Zurich, Switzerland.

4Max-Planck-Institut für Astronomie, 69117 Heidelberg, Germany.

5Instituto de Astrofísica de Canarias, E-38205 La Laguna, Tenerife, Spain.

6Departamento de Astrofísica, Universidad de La Laguna, E-38206 La Laguna, Tenerife, Spain.

7Physikalisches Institut, University of Bern, 3012 Bern, Switzerland.

8European Southern Observatory, Alonso de Córdova 3107, Vitacura, Región Metropolitana, Chile.

9Center for Cosmology and Astrophysics, Alikhanian National Science Laboratory, 0036 Yerevan, Armenia.

10Department of Physics, School of Medicine, Kurume University, Fukuoka 830-0011, Japan.

11National Astronomical Observatory, Mitaka, Tokyo 181-8588, Japan.

12Sōgō kenkū daigakuin daigaku, The Graduate University for Advanced Studies, Mitaka, Tokyo 181-8588, Japan.

13Instituto de Astronomía, Universidad Nacional Autónoma de México, Ciudad Universitaria, Ciudad de México, C.P. 04510, México.

14Observatorio Astronómico de Córdoba, Universidad Nacional de Córdoba, X5000BGR Córdoba, Argentina.

15Consejo Nacional de Investigaciones Científicas y Técnicas, C1425FQB Buenos Aires, Argentina.

16Institut d'Astrophysique de Paris, UMR7095 Centre national de la recherche scientifique, Sorbonne Université, 75014 Paris, France.

17Laboratório Nacional de Astrofísica, Itajubá MG 37504-364, Brazil.

***Corresponding author. Email: vadibekyan@astro.up.pt**

REFERENCES AND NOTES

1. S. G. Sousa *et al., Astron. Astrophys.* **487**, 373–381 (2008).

2. Materials and methods are available as supplementary materials.

3. B. J. Fulton *et al., Astron. J.* **154**, 109 (2017).

4. J. E. Owen, Y. Wu, *Astrophys. J.* **847**, 29 (2017).

5. S. Ginzburg, H. E. Schlichting, R. Sari, *Mon. Not. R. Astron. Soc.* **476**, 759–765 (2018).

6. S. Jin, C. Mordasini, *Astrophys. J.* **853**, 163 (2018).

7. J. Venturini, O. M. Guilera, J. Haldemann, M. P. Ronco, C. Mordasini, *Astron. Astrophys.* **643**, L1 (2020).

8. A. Dotter, C. Conroy, P. Cargile, M. Asplund, *Astrophys. J.* **840**, 99 (2017).

9. M. Asplund, N. Grevesse, A. J. Sauval, P. Scott, *Annu. Rev. Astron. Astrophys.* **47**, 481–522 (2009).

10. J. C. Bond, D. P. O'Brien, D. S. Lauretta, *Astrophys. J.* **715**, 1050–1070 (2010).

11. A. Thiabaud *et al., Astron. Astrophys.* **562**, A27 (2014).

12. A. Bonsor *et al., Mon. Not. R. Astron. Soc.* **503**, 1877–1883 (2021).

13. C. Dorn *et al., Astron. Astrophys.* **577**, A83 (2015).

14. C. T. Unterborn, E. E. Dismukes, W. R. Panero, *Astrophys. J.* **819**, 32 (2016).

15. K. Lodders, *Astrophys. J.* **591**, 1220–1247 (2003).

16. N. C. Santos *et al., Astron. Astrophys.* **580**, L13 (2015).

17. N. C. Santos *et al., Astron. Astrophys.* **608**, A94 (2017).

18. C. Dorn *et al., Astron. Astrophys.* **597**, A37 (2017).

19. J. E. Owen, *Annu. Rev. Earth Planet. Sci.* **47**, 67–90 (2019).

20. D. C. Rubie *et al., Icarus* **248**, 89–108 (2015).

21. M. Plotnykov, D. Valencia, *Mon. Not. R. Astron. Soc.* **499**, 932–947 (2020).

22. A. Aguichine, O. Mousis, B. Devouard, T. Ronnet, *Astrophys. J.* **901**, 97 (2020).

23. R. A. Marcus, D. Sasselov, L. Hernquist, S. T. Stewart, *Astrophys. J.* **712**, L73–L76 (2010).

24. J. G. Schulze *et al., Planet. Sci. J.* **2**, 113 (2021).

25. J. Scora, D. Valencia, A. Morbidelli, S. Jacobson, *Mon. Not. R. Astron. Soc.* **493**, 4910–4924 (2020).

26. G. Lacedelli *et al., Mon. Not. R. Astron. Soc.* **501**, 4148–4166 (2021).

27. J. Lillo-Box *et al., Astron. Astrophys.* **640**, A48 (2020).

28. A. Mortier *et al., Mon. Not. R. Astron. Soc.* **499**, 5004–5021 (2020).

29. B. Bitsch, C. Battistini, *Astron. Astrophys.* **633**, A10 (2020).

30. V. Adibekyan, abg8794_spectra_DataS1.zip, Figshare (2021);
https://doi.org/10.6084/m9.figshare.16451166.v1.

ACKNOWLEDGMENTS

V.A. thanks A. Tajitsu for reducing the High Dispersion Spectrograph spectra. Based on data collected at the Subaru Telescope (program ID S16B0178S; principal investigator: V.A.), which is operated by the National Astronomical Observatory of Japan. We are honored and grateful for the opportunity of observing the Universe from Maunakea, which has great cultural, historical, and natural significance in Hawaii. This research is also partly based on observations (program ID GN-2017A-FT-20; principal investigator: E.J.) obtained at the international Gemini Observatory, a program of NSF's NOIRLab, which is managed by the Association of Universities for Research in Astronomy (AURA) under a cooperative agreement with the NSF on behalf of the Gemini Observatory partnership: the NSF (United States), National Research Council (Canada), Agencia Nacional de Investigación y Desarrollo (Chile), Ministerio de Ciencia, Tecnología e Innovación (Argentina), Ministério da Ciência, Tecnologia, Inovações e Comunicações (Brazil), and Korea Astronomy and Space Science Institute (Republic of Korea). This research is also based on observations collected at the European Southern Observatory (ESO) under ESO programs listed in table S1. This work has made use of data from the European Space Agency (ESA) mission (Gaia), processed by the Gaia

Data Processing and Analysis Consortium (DPAC). Funding for DPAC has been provided by national institutions, specifically the institutions participating in the Gaia Multilateral Agreement. This research used the facilities of the Italian Center for Astronomical Archive (IA2) operated by INAF at the Astronomical Observatory of Trieste; the NASA Exoplanet Archive, which is operated by the California Institute of Technology, under contract with NASA under the Exoplanet Exploration Program; and the SIMBAD database, operated at CDS, Strasbourg, France. **Funding:** V.A., S.G.S., N.C.S., S.C.C.B., E.D.M., O.D.S.D., and J.P.F. were supported by Fundação para a Ciência e Tecnologia (FCT) through national funds and by FEDER through COMPETE2020 - Programa Operacional Competitividade e Internacionalização by these grants: UID/FIS/04434/2019, UIDB/04434/2020, UIDP/04434/2020, PTDC/FIS-AST/32113/2017 and POCI-01-0145-FEDER-032113, and PTDC/FIS-AST/28953/2017 and POCI-01-0145-FEDER-028953. V.A., E.D.M., N.C.S., and S.G.S. acknowledge support from FCT through Investigador FCT contracts IF/00650/2015/CP1273/CT0001, IF/00849/2015/CP1273/CT0003, IF/00169/2012/CP0150/CT0002, and IF/00028/2014/CP1215/CT0002, respectively, and POPH/FSE (EC) by FEDER funding through the program “Programa Operacional de Factores de Competitividade - COMPETE.” C.D. acknowledges support from the Swiss National Science Foundation (SNSF) under grant PZ00P2_174028. C.D. and C.M. acknowledge support from the National Center for Competence in Research PlanetS supported by the SNSF. O.D.S.D. and J.P.F. are supported by contracts (DL 57/2016/CP1364/CT0004 and DL57/2016/CP1364/CT0005, respectively) funded by FCT. E.M. acknowledges funding from the French National Research Agency (ANR) under contract ANR-18-CE31-0019 (SPlaSH). B.B. was supported by the European Research Council (ERC Starting Grant 757448-PAMDORA). **Author contributions:** V.A. led the data analysis and wrote the paper, with contributions from C.D. C.D. led the planetary interior analysis, and S.G.S. performed the stellar parameter analysis. V.A. determined the composition of the stars, with contributions from E.D.M. N.C.S., B.B., C.M., B.M.T.B.S., and G.I. contributed to the discussion of the implications of the data. S.C.C.B., O.D.S.D., A.A.H., and M.O. contributed to the general discussion of the results. C.D., S.G.S., N.C.S., G.I., C.M., E.D.M., M.K., Y.T., E.J., R.P., and E.M. gathered the spectroscopic observations. J.P.F. and P.F. performed the statistical analysis. All authors discussed the results and commented on the manuscript. **Competing interests:** The authors declare no competing interests. **Data and materials availability:** The archival observations used were obtained from the sources listed in table S1. Our own observations are available in the following observatory archives: the Gemini Observatory Archive at

https://archive.gemini.edu/searchform under program ID GN-2017A-FT-20 and the Subaru Mitaka Okayama Kiso Archive at **https://smoka.nao.ac.jp/objectSearch.jsp** by selecting Subaru HDS, then searching for Kepler-20 and Kepler-78. Our final co-added spectra for all stars in the sample are available on Figshare (*30*). The Python code we used to calculate star iron is provided in data S1. The output values for the properties of the stars and exoplanets are listed in tables S3 and S4, respectively. The numerical values of the correlations we found using ODR are listed in tables S6 and S7.

10.1126/science.abg8794

SUPPLEMENTARY MATERIALS

science.org/doi/10.1126/science.abg8794

Materials and Methods

Supplementary Text Figs. S1 to S4

Tables S1 to S8

References (*31*–*96*)

Data S1

10 February 2021; accepted 27 August 2021